

Supporting Information

**Black Glasses Grafted Micron Silicon: A Resilient Anode
Material for High Performance Lithium-ion Batteries**

Ravi Nandan,^a Noriyuki Takamori,^a Koichi Higashimine,^b Rajashekar Badam,^a Noriyoshi

Matsumi^{a,*}

^aGraduate School of Advanced Science and Technology,

Japan Advanced Institute of Science and Technology,

^bCenter for Nano Materials and Technology,

Japan Advanced Institute of Science and Technology,

*E-mail: - matsumi@jaist.ac.jp (Prof. Noriyoshi Matsumi)

Tel: +81-761-51-1600

Experimental Section

Materials

Micron sized silicon particles (purchased from SkySpring Nanomaterials, Inc. Houston), dopamine i.e. 3-Hydroxytyramine Hydrochloride (>98%, purchased from TCI Co. Ltd.) (3-Aminopropyl)triethoxysilane solution (APTES, 99%, purchased from Sigma Aldrich). The commercially available binders like sodium carboxymethyl cellulose (CMC, average molecular weight~250000) and Poly(acrylic acid)(PAA) were procured from Sigma-Aldrich and has been used for slurry preparation in equal proportion. 1.0 M Tris-HCl buffer solution of pH 8.5 was obtained from Nippon Gene, Japan and has been used to explore the dopamine polymerization chemistry. For the conductive support material acetylene black (AB) purchased from Denka Japan Private Co., Ltd was used during slurry preparation. Carbon nano tubes powder was obtained from Zeon Nano Technology Co. Ltd., Japan. The battery grade copper foil (thickness~ 20 μm) which was obtained from the Nilaco corporation was used for slurry casting and as anode current collector. During cell fabrication, 1.0 M commercially available lithium hexafluorophosphate (LiPF_6) in EC/DEC=50/50 (V/V) solution was used as

electrolyte. The all chemicals/materials were used as received. The commercially available “Celgard 2500 polypropylene” separator was used in cell fabrication.

Synthesis

- Step 1

Silicon micron particles (SiMP ~ 8gm) were dispersed in an aqueous solution of Milli Q water and methanol (water : methanol :: 1 : 1). This solution was subjected to sonication (1 h) followed by overnight stirring. Next, the pH of solution was controlled to 8.5 by tris-buffer solution. This solution was further sonicated and subsequently stirred for 30 min, each.

Following this, the commercially available dopamine (3-Hydroxytyramine Hydrochloride) powder was introduced in this solution and stirred for 48 h for uniform mixing. The colour of the overall solution changes from yellowish-brown to black with time, indicating the polymerization of dopamine to polydopamine as at 8.5 pH the dopamine goes self-polymerization to polydopamine.^{1,2} The excellent adhesive nature of polydopamine ensures the formation of polydopamine coated SiMP.

Next, the solvent from the solution was removed and the obtained (polydopamine coated SiMP) powder was subjected to heat treatment in nitrogen ambience at 800 degrees Celsius for 2 h. The obtained material post heat treatment was

the carbon coated SiMP and named as Si/C Figure S1.

- Step 2

The Si/C powder developed in 1st step was then introduced in an aqueous dispersion of acetylene black (AB) and (3-Aminopropyl)triethoxysilane (APTES) solution. This solution was then stirred for 6 h and sonicated for 1 h. Finally, the solvent was removed from this solution of AB + APTES + Si/C and the obtained powder was crushed appropriately with mortar-pestle and subjected to heat treatment at 1000 °C for 10 h in nitrogen ambiance. The final product obtained was silicon oxycarbide (SiC_xO_y) black glasses (BG) grafted SiMP anode material.

This final product was named as Si/C/ABG (Figure 1 in main manuscript) where ABG indicates acetylene black (AB) embedded Silicon oxycarbide black glasses. The APTES was the precursor for silicon oxycarbide (SiC_xO_y) black glasses

Characterization

For the structural characterization we have employed the transmission electron microscopy (TEM equipment from Hitachi HF-2000), X-ray diffraction (XRD equipment from SmartLab X-ray diffractometer, Rigaku), X-ray photoelectron spectroscopy (XPS equipment from S-probe Surface Spectrometer),

thermogravimetric analysis (TGA equipment from STA 7200 Thermal Analysis System, HITACHI) and scanning electron microscopy (SEM equipment from Hitachi S-4500)

The estimation of nitrogen atomic percentage (at. %) in Si/C/ABG from XPS study was carried out by integrating the area under the curve of high resolution (HR) XPS spectrum (Figure S3). The obtained area under curves were further normalized with the sensitivity factor (SF, equation S1) of respective elements present in the composite.²⁻⁴

$$\text{Elemental at. \%} = \frac{\frac{A_t}{SF_t}}{\sum_t \frac{A_t}{SF_t}} * 100 \quad (\text{S1})$$

Where,

t = Si/C /N/O

SF_{Si} = 0.27

SF_C = 0.25;

SF_N = 0.42;

SF_O = 0.66

For the electrochemical screening of anodic/cathodic half-cells as well as Si/C/ABG based full-cells, BSC-805 and Bio Logic Science Instrument electrochemical stations were used. For the cell fabrications MBRAUN LABSTAR glove box facility was used and standard cell fabrication protocols were religiously followed. The oxygen and moisture concentrations were maintained below 0.5 ppm in glove box facility. The ball-milling equipment from FRITSCH – Premium line, Pulverisette 7, was used for slurries preparation. To monitor the volumetric expansion of anode materials the HS cell from EC Frontier Co. Ltd., Japan, was used.

Slurry and electrode preparation

The slurries of various anode materials (e.g., SiMP, Si/BG and Si/C/ABG) were prepared using carboxymethyl cellulose (CMC) and polyacrylic acid (PAA) traditional binders. The CMC and PAA were used in equal proportion. The acetylene black (AB) was used as conductive support. The Milli-Q water (resistivity $\sim 18.2 \text{ M}\Omega\cdot\text{cm}$) was used as solvent. The slurry was casted on battery grade copper foil and dried at 80 °C followed by appropriate roll press at 80 °C. The half as well as full-cell studies were carried out using CR2025 coin cells. The commercially

available lithium foil was used as the counter as well as reference electrodes for anodic and cathodic half-cell studies. Table S1 summarizes the slurry preparation conditions used in this study.

Table S1. The conditions used in slurry preparation for present study

Materials	Weight %
Active material (Si/C/ABG, Si/Bg or SiMP)	70
CMC	7.5
PAA	7.5
Acetylene black	15

For comparatively high loading study, during slurry preparation 2.5 wt.% of SWCNT as a conductive support was used alongside 12.5 wt.% of traditionally used acetylene black. The SWCNT are known for their excellent electrical conductivity and can be useful with increased thickness of anode material film on current collector.

Table S2. The conditions used in slurry preparation for high loading study

Materials	Weight %
Active material (Si/C/ABG)	70
CMC	7.5
PAA	7.5
Acetylene black	12.5
Single wall carbon nanotubes (SWCNT)	2.5

Full-cell assembly

For the fabrication of full-cell, commercially available Lithium Nickel-Cobalt-Aluminum Oxide (NCA) cathode was used as the counter electrode. These NCA electrodes were pre-cycled initially for few cycles in cathodic half-cell configuration. Similarly, the Si/C/ABG based anode electrodes aimed to use in full-cell as negative electrodes were also pre-cycled to minimize the possible initial Li⁺-ions losses. These respective activated cathode and anode electrodes were used to assemble the final full-cells.

Moreover, to realize the full cell with maximum possible efficacy, the capacity matching and hence the active material loading was optimized in light to equation S2.^{5,6}

$$\frac{C_{Anode} * M_{Anode}}{C_{Cathode} * M_{Cathode}} \geq 1 \quad (S2)$$

Where,

$C_{Anode} / C_{Cathode}$ are respective specific capacities,

$M_{Anode} / M_{Cathode}$ are respective active material loading.

***Ex-situ* post cyclic studies**

For post cycling studies, the cycled half-cells (in delithiated state) were cautiously dismantled inside the glove box and the respective anodes were recovered (Si/C/ABG or SiMP, post rate studies i.e. after 65th cycle in delithiated state). These recovered anode electrodes were then subsequently transferred to the scanning electron microscopy and X-ray photoelectron facilities with utmost care for further studies.

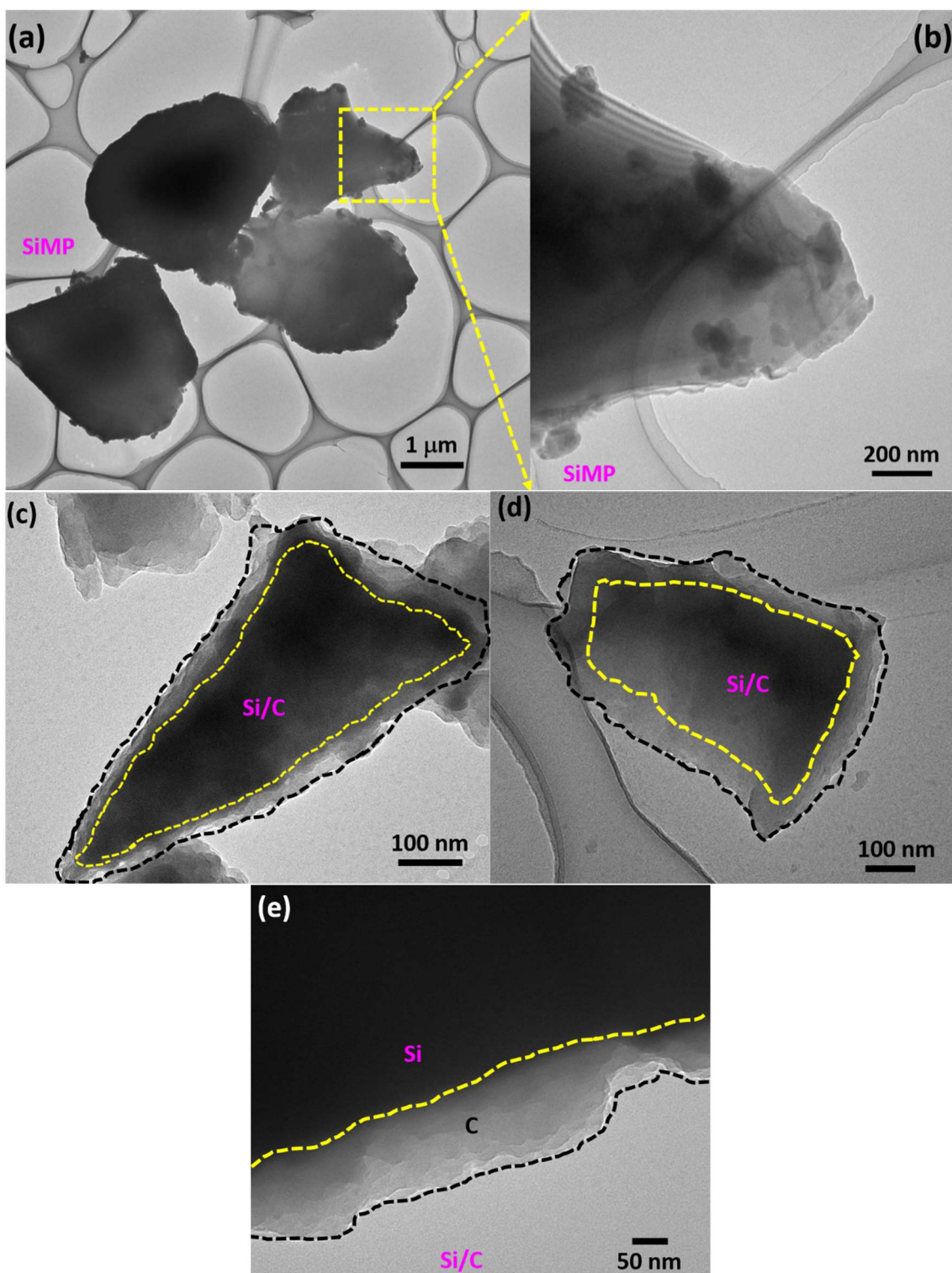


Figure S1. Bright field TEM images of (a,b) pristine micron silicon particles (SiMP) and (c-e) carbon coated SiMP (Si/C).

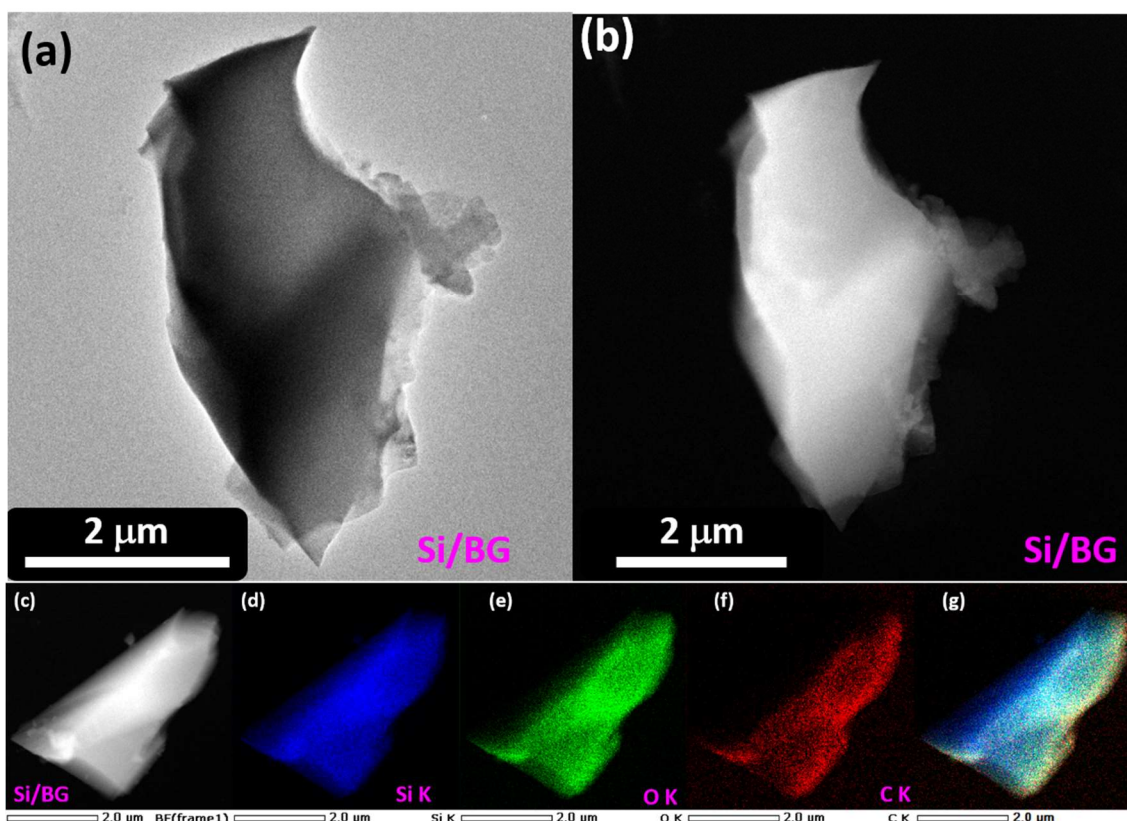


Figure S2. (a) Bright field TEM image of silicon oxycarbide black glasses (BG) coated SiMP i.e. Si/BG. (b) HAADF-STEM image of Si/BG. (c) HAADF-STEM image of Si/BG subjected to elemental portioning, (d-f) respective elemental mapping and (g) the combined image deduced from overlapping of Figure d-f.

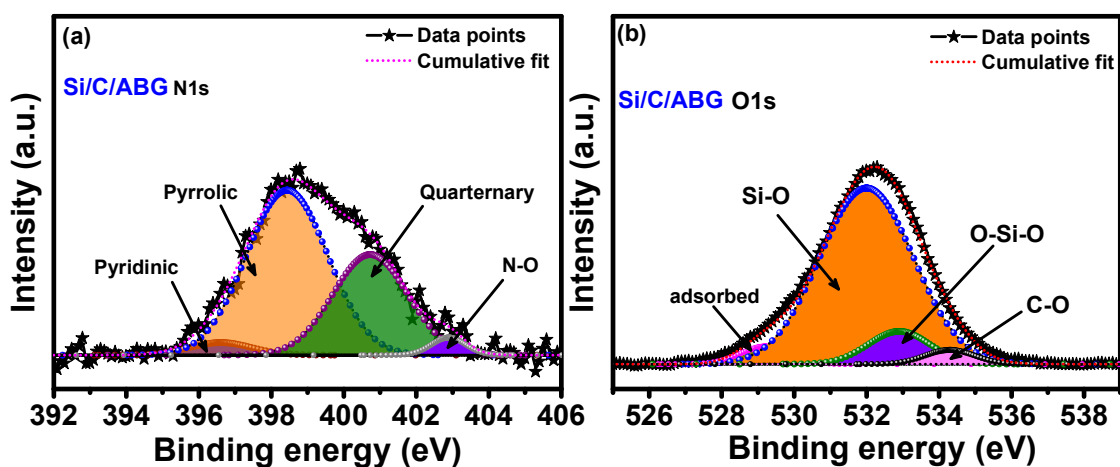


Figure S3. The deconvoluted HRXPS spectra of (a) N 1s and, (b) O 1s for Si/C/ABG

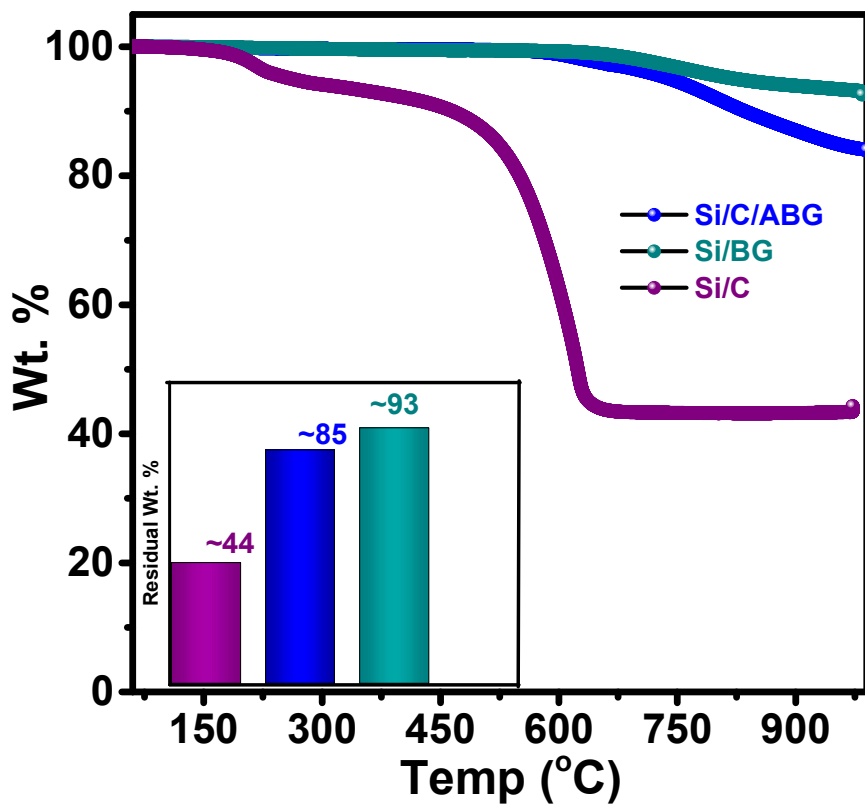


Figure S4. TGA profiles for Si/C/ABG, Si/BG and Si/C in oxygen ambiance. The temperature ramping rate was 5 °C/min.

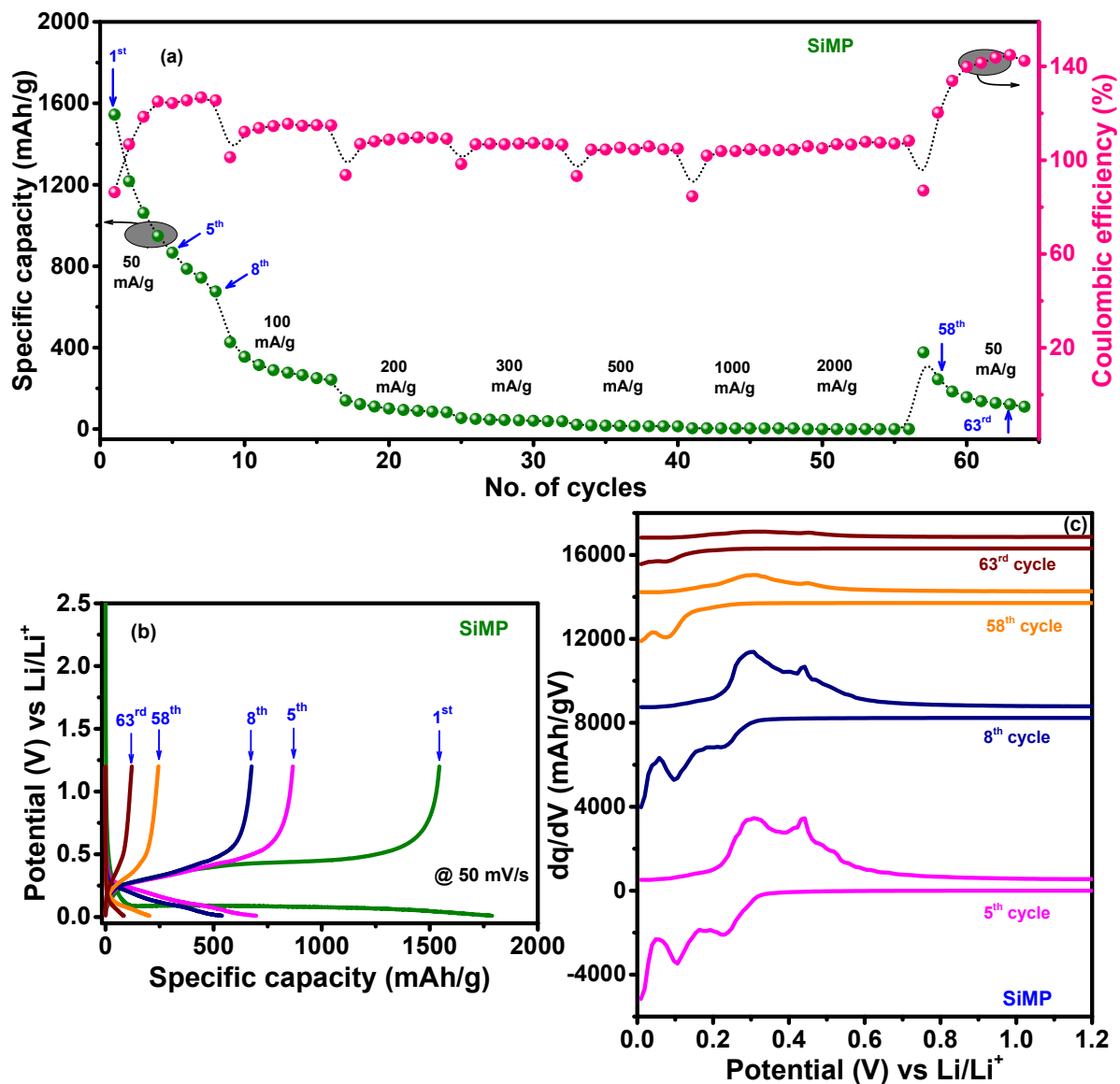


Figure S5. (a) Rate studies (b) lithiation-delithiation voltage profiles for selected cycles as indicated by blue arrows in Figure S4a, (c) the concomitant differential capacity profiles deduced from lithiation-delithiation voltage profiles in Figure S4b for as-received micron Si particle (SiMP) anode.

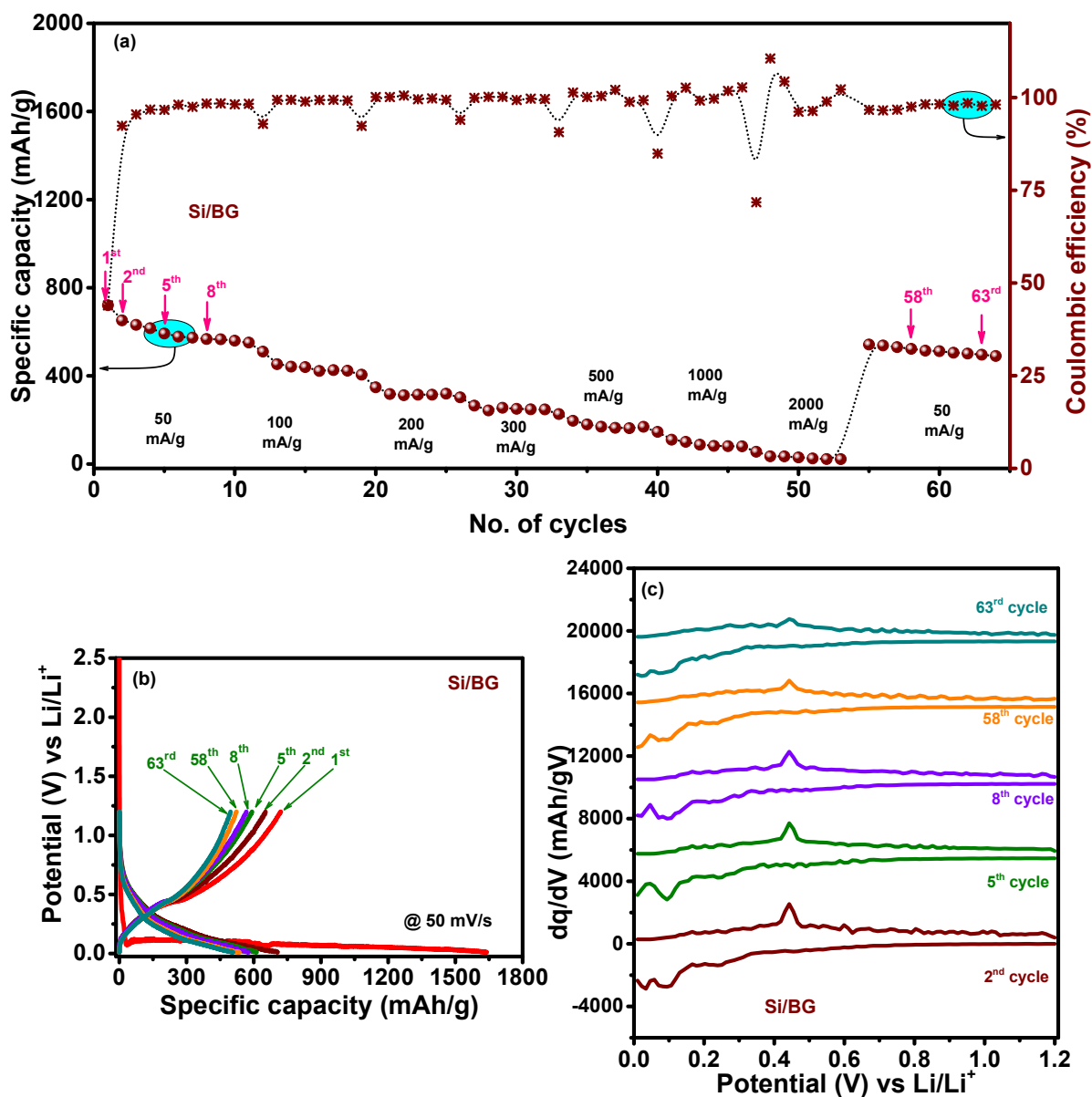


Figure S6. (a) Rate studies (b) lithiation-delithiation voltage profiles for selected cycles as indicated by pink arrows in Figure S5a, (c) the concomitant differential capacity profiles deduced from lithiation-delithiation voltage profiles in Figure S5b for silicon oxycarbide black glasses (BG) modified SiMP i.e., Si/BG anode.

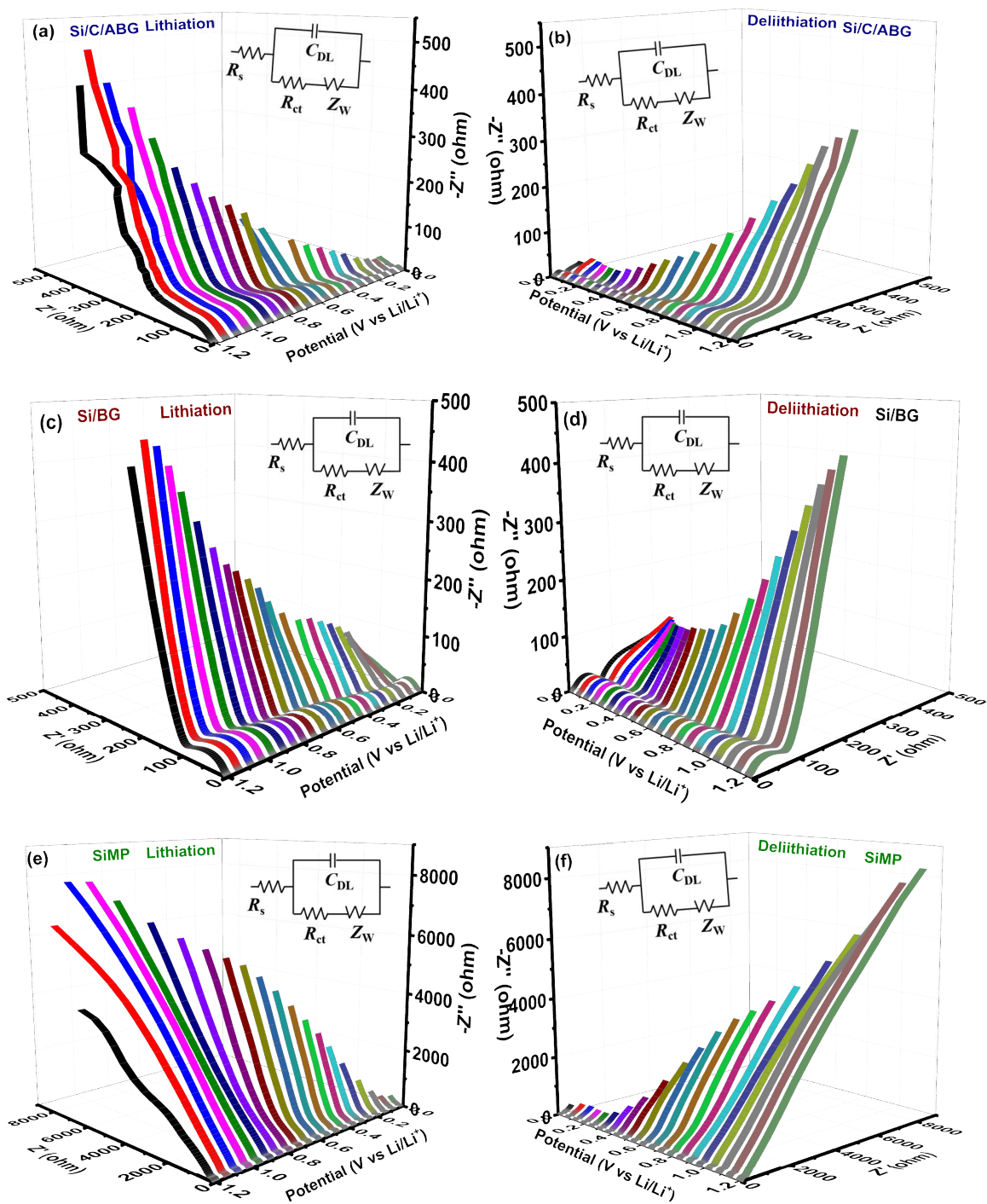


Figure S7. DEIS profiles over lithiation - delithiation potential windows on (a,b) Si/C/ABG, (c,d) Si/BG and, (e) SiMP anodes, post their respective rate studies (after ~65th cycle). The inset shows the circuit fitting used for individual EIS in DEIS.

Table S3a: DEIS circuit analysis report for Si/C/ABG during lithiation deduced from Figure S7a.

Lithiation potential (V vs Li/Li ⁺)	R _s	C _{DL}	R _{ct}	Z _w	Circuit
0.010	5.464	1.23E-05	20.11	0.08701	R(C(RW))
0.070	5.194	1.45E-05	15.7	0.08272	R(C(RW))
0.070	5.209	1.88E-05	14.58	0.06653	R(C(RW))
0.129	5.462	2.16E-05	15.5	0.05131	R(C(RW))
0.188	5.839	2.03E-05	19.77	0.04377	R(C(RW))
0.248	6.155	1.98E-05	25.08	0.03914	R(C(RW))
0.307	15.96	2.87E-05	42.96	0.02851	R(C(RW))
0.367	3.714	5.08E-06	46.42	0.0259	R(C(RW))
0.426	6.796	1.74E-05	40.93	0.02833	R(C(RW))
0.486	3.818	5.56E-06	45.72	0.02619	R(C(RW))
0.545	3.847	5.82E-06	45.79	0.02631	R(C(RW))
0.605	7.123	1.50E-05	55.44	0.01914	R(C(RW))
0.665	7.194	1.45E-05	59.02	0.01702	R(C(RW))
0.725	7.232	1.41E-05	61.86	0.01498	R(C(RW))
0.784	7.196	1.34E-05	63.15	0.01288	R(C(RW))
0.843	7.254	1.28E-05	66.02	0.01064	R(C(RW))
0.903	7.126	1.19E-05	65.43	0.008961	R(C(RW))
1.022	6.938	1.09E-05	63.47	0.007815	R(C(RW))
1.082	6.789	1.01E-05	62.69	0.006984	R(C(RW))
1.142	6.654	9.53E-06	61.3	0.006514	R(C(RW))
1.200	6.537	9.21E-06	60.11	0.007118	R(C(RW))

Table S3b: DEIS circuit analysis report for Si/C/ABG during delithiation deduced from Figure S7b

Delithiation potential (V vs Li/Li ⁺)	R _s	C _{DL}	R _{ct}	Z _w	Circuit
0.010	5.932	1.25E-05	26.76	0.06362	R(C(RW))
0.070	6.012	1.19E-05	27.52	0.04895	R(C(RW))

0.070	6.09	1.14E-05	28.38	0.05598	R(C(RW))
0.129	5.98	1.01E-05	27.64	0.06396	R(C(RW))
0.188	5.74	8.41E-06	25.88	0.06962	R(C(RW))
0.248	5.51	6.93E-06	24.03	0.06818	R(C(RW))
0.307	5.304	5.54E-06	23.5	0.0564	R(C(RW))
0.367	5.126	4.54E-06	23.53	0.04514	R(C(RW))
0.426	5.04	3.98E-06	24.3	0.03681	R(C(RW))
0.486	5.123	3.76E-06	27.1	0.03166	R(C(RW))
0.545	5.306	3.92E-06	30.98	0.02913	R(C(RW))
0.605	5.616	4.40E-06	36.17	0.02645	R(C(RW))
0.665	5.919	4.87E-06	41.18	0.02303	R(C(RW))
0.725	6.161	5.29E-06	45.47	0.01948	R(C(RW))
0.784	6.23	5.39E-06	47.45	0.01615	R(C(RW))
0.843	6.383	5.50E-06	50.52	0.01339	R(C(RW))
0.903	6.469	5.48E-06	52	0.01157	R(C(RW))
1.022	6.518	5.44E-06	53.26	0.01028	R(C(RW))
1.082	6.521	5.40E-06	53.36	0.009366	R(C(RW))
1.142	6.541	5.35E-06	54.12	0.00879	R(C(RW))
1.200	6.498	5.21E-06	54.35	0.008304	R(C(RW))

Table S4a: DEIS circuit analysis report for Si/BG during lithiation deduced from Figure S7c

Lithiation potential (V vs Li/Li⁺)	R_s	C_{DL}	R_{ct}	Z_w	Circuit
0.010	3.543	4.53E-06	45.93	0.02782	R(C(RW))
0.070	3.963	6.92E-06	38.73	0.02927	R(C(RW))
0.070	4.249	8.89E-06	38.76	0.02957	R(C(RW))
0.129	4.347	9.67E-06	40.38	0.02852	R(C(RW))
0.188	4.408	9.94E-06	43.57	0.02805	R(C(RW))
0.248	4.465	9.97E-06	48.2	0.02787	R(C(RW))
0.307	4.456	9.98E-06	49.56	0.02648	R(C(RW))
0.367	4.533	1.01E-05	53.99	0.0253	R(C(RW))
0.426	4.55	9.98E-06	57.55	0.02348	R(C(RW))
0.486	4.528	9.75E-06	59.6	0.02109	R(C(RW))
0.545	4.47	9.47E-06	60.12	0.01928	R(C(RW))
0.605	4.428	9.32E-06	60.43	0.01819	R(C(RW))
0.665	4.342	9.18E-06	58.61	0.01725	R(C(RW))
0.725	4.276	9.03E-06	57.36	0.01638	R(C(RW))
0.784	4.264	8.87E-06	58.03	0.01479	R(C(RW))
0.843	4.223	8.60E-06	58.13	0.0131	R(C(RW))
0.903	4.19	8.38E-06	58.41	0.01175	R(C(RW))
1.022	4.18	8.22E-06	59.05	0.01084	R(C(RW))
1.082	4.196	8.15E-06	59.89	0.01027	R(C(RW))
1.142	4.168	8.11E-06	58.16	0.01019	R(C(RW))
1.200	4.145	8.21E-06	54.48	0.01122	R(C(RW))

Table S4b: DEIS circuit analysis report for Si/BG during delithiation deduced from Figure S7d

Delithiation potential (V vs Li/Li⁺)	R_s	C_{DL}	R_{ct}	Z_w	Circuit
0.010	3.564	4.20E-06	54.06	0.01778	R(C(RW))
0.070	3.584	4.23E-06	55.29	0.01766	R(C(RW))
0.070	3.587	4.32E-06	57.21	0.0198	R(C(RW))
0.129	3.702	4.57E-06	56.99	0.0217	R(C(RW))

0.188	3.655	4.58E-06	54.79	0.02301	R(C(RW))
0.248	3.676	4.73E-06	51.83	0.02416	R(C(RW))
0.307	15.96	2.87E-05	42.96	0.02851	R(C(RW))
0.367	3.714	5.08E-06	46.42	0.0259	R(C(RW))
0.426	3.772	5.38E-06	44.78	0.0264	R(C(RW))
0.486	3.818	5.56E-06	45.72	0.02619	R(C(RW))
0.545	3.847	5.82E-06	45.79	0.02631	R(C(RW))
0.605	3.863	6.08E-06	45.41	0.02522	R(C(RW))
0.665	3.869	6.22E-06	45.2	0.02319	R(C(RW))
0.725	3.852	6.31E-06	44.71	0.0209	R(C(RW))
0.784	3.852	6.40E-06	44.91	0.01851	R(C(RW))
0.843	3.86	6.46E-06	44.82	0.01648	R(C(RW))
0.903	3.833	6.52E-06	43.99	0.01484	R(C(RW))
1.022	3.89	6.63E-06	45.99	0.01353	R(C(RW))
1.082	3.91	6.69E-06	47.11	0.01261	R(C(RW))
1.142	3.921	6.73E-06	47.95	0.01192	R(C(RW))
1.200	3.846	6.68E-06	45.94	0.01154	R(C(RW))

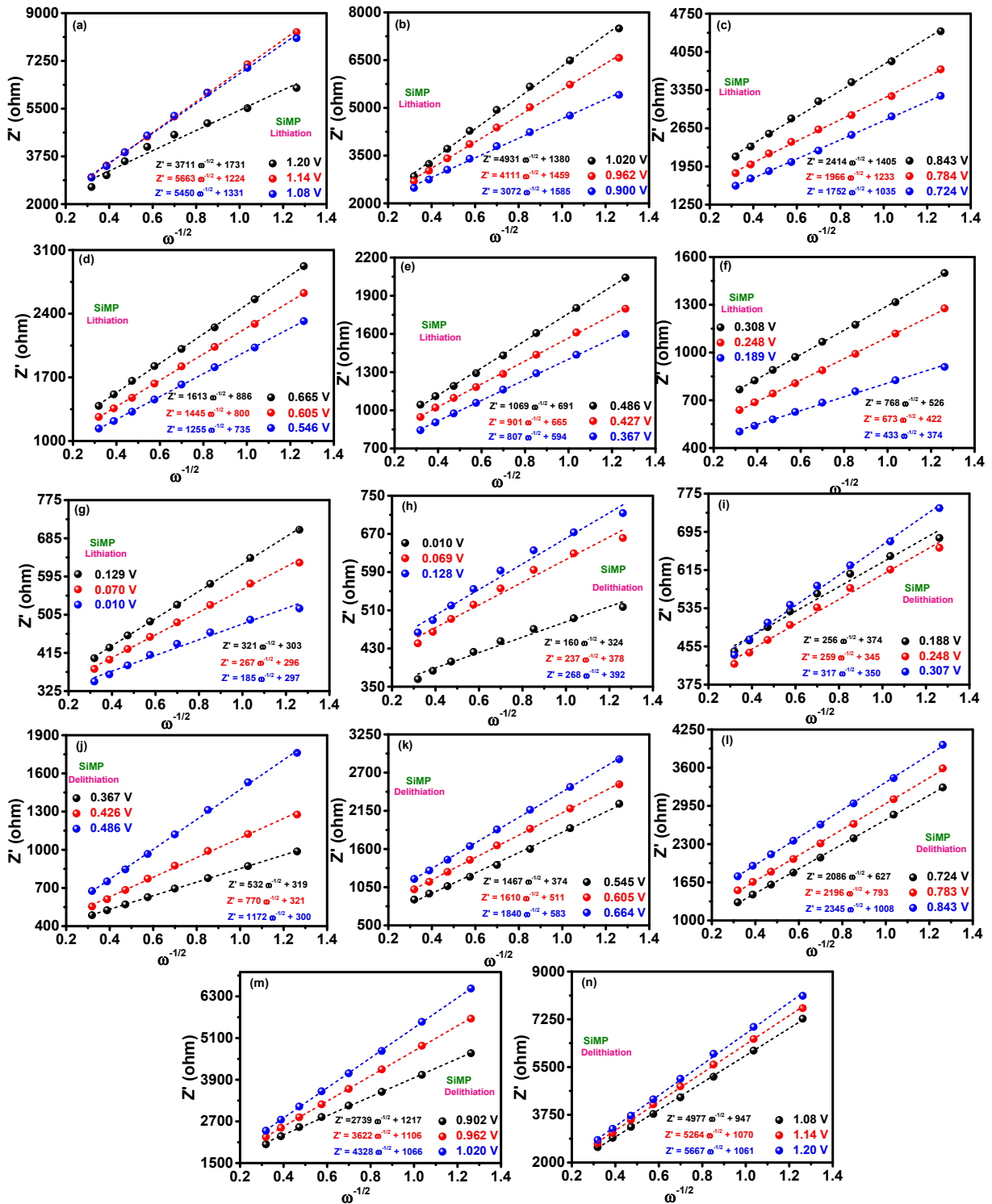
Table S5a: DEIS circuit analysis report for SiMP during lithiation deduced from Figure S7e

Lithiation potential (V vs Li/Li⁺)	R_s	C_{DL}	R_{ct}	Z_w	Circuit
0.010	3.163	1.65E-06	128.4	0.006114	R(C(RW))
0.070	3.161	1.67E-06	111	0.004906	R(C(RW))
0.070	3.17	1.69E-06	106.2	0.004214	R(C(RW))
0.129	3.163	1.65E-06	110	0.002945	R(C(RW))
0.188	3.128	1.54E-06	139.4	0.002034	R(C(RW))
0.248	3.121	1.49E-06	165	0.001591	R(C(RW))
0.307	3.107	1.49E-06	163.8	0.001341	R(C(RW))
0.367	3.087	1.48E-06	160.4	0.001165	R(C(RW))
0.426	3.087	1.47E-06	159.2	0.001022	R(C(RW))
0.486	3.087	1.45E-06	157.4	0.000905	R(C(RW))
0.545	3.08	1.44E-06	152.8	0.000812	R(C(RW))
0.605	3.059	1.43E-06	143.1	0.000746	R(C(RW))
0.665	3.039	1.42E-06	135.3	0.000675	R(C(RW))
0.725	3.021	1.40E-06	125.9	0.00061	R(C(RW))
0.784	3.022	1.38E-06	120.3	0.00054	R(C(RW))
0.843	2.993	1.36E-06	107.2	0.000484	R(C(RW))
0.903	2.979	1.33E-06	98.34	0.000441	R(C(RW))
1.022	2.946	1.32E-06	87.4	0.000414	R(C(RW))
1.082	2.946	1.31E-06	84.12	0.0004	R(C(RW))
1.142	2.934	1.31E-06	82.84	0.000418	R(C(RW))
1.200	2.994	1.35E-06	102.8	0.000511	R(C(RW))

Table S5b: DEIS circuit analysis report for SiMP during delithiation deduced from Figure S7f.

Delithiation potential (V vs Li/Li⁺)	R_s	C_{DL}	R_{ct}	Z_w	Circuit
0.010	3.213	1.67E-06	139.4	0.006056	R(C(RW))
0.070	3.225	1.67E-06	142.1	0.004516	R(C(RW))
0.070	3.225	1.68E-06	145.2	0.004141	R(C(RW))

0.129	3.236	1.69E-06	147.9	0.004422	R(C(RW))
0.188	3.218	1.71E-06	140.3	0.004841	R(C(RW))
0.248	3.191	1.69E-06	131	0.004379	R(C(RW))
0.307	3.175	1.64E-06	121.4	0.003477	R(C(RW))
0.367	3.149	1.58E-06	112.7	0.002727	R(C(RW))
0.426	3.109	1.50E-06	113.6	0.002054	R(C(RW))
0.486	3.092	1.43E-06	132.4	0.001504	R(C(RW))
0.545	3.083	1.42E-06	144.4	0.001218	R(C(RW))
0.605	3.071	1.42E-06	147.3	0.001022	R(C(RW))
0.665	3.066	1.41E-06	144.9	0.00089	R(C(RW))
0.725	3.057	1.40E-06	138.3	0.000781	R(C(RW))
0.784	3.02	1.39E-06	124.4	0.000695	R(C(RW))
0.843	3.025	1.37E-06	119.3	0.000612	R(C(RW))
0.903	3.016	1.35E-06	112.2	0.000551	R(C(RW))
1.022	2.998	1.34E-06	103.8	0.000504	R(C(RW))
1.082	2.982	1.32E-06	97.48	0.000469	R(C(RW))
1.142	2.944	1.31E-06	88.05	0.000443	R(C(RW))
1.200	2.944	1.29E-06	85.74	0.00042	R(C(RW))



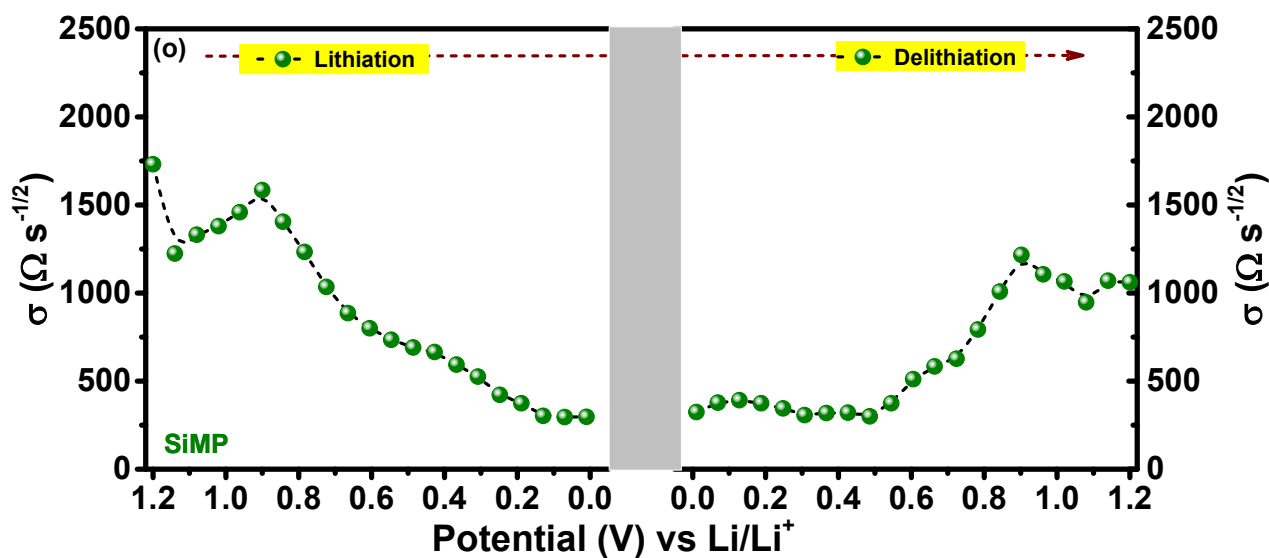
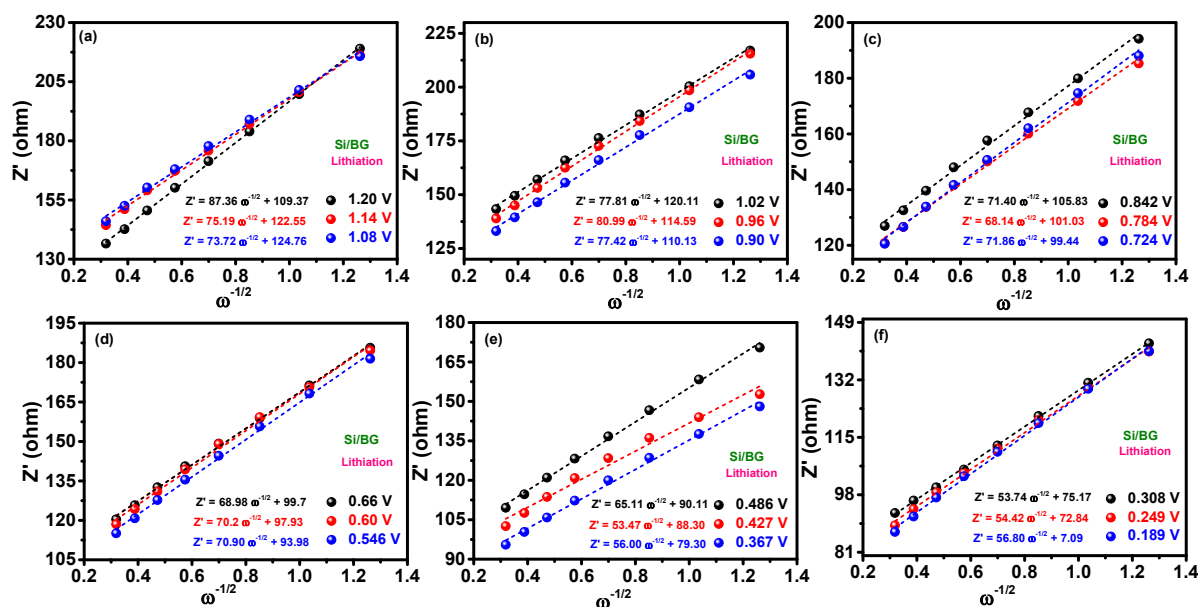


Figure S8. The Warburg plots for lithiation (a-g) and delithiation (h-n), construed from low frequency region of each Nyquist plots in DEIS spectra (Figure S6) of SiMP, post rate study (after $\sim 65^{\text{th}}$ cycle). (o) Warburg coefficient, σ , variation of SiMP anode over lithiation – delithiation potential window, deduced from the slope of Warburg plots.



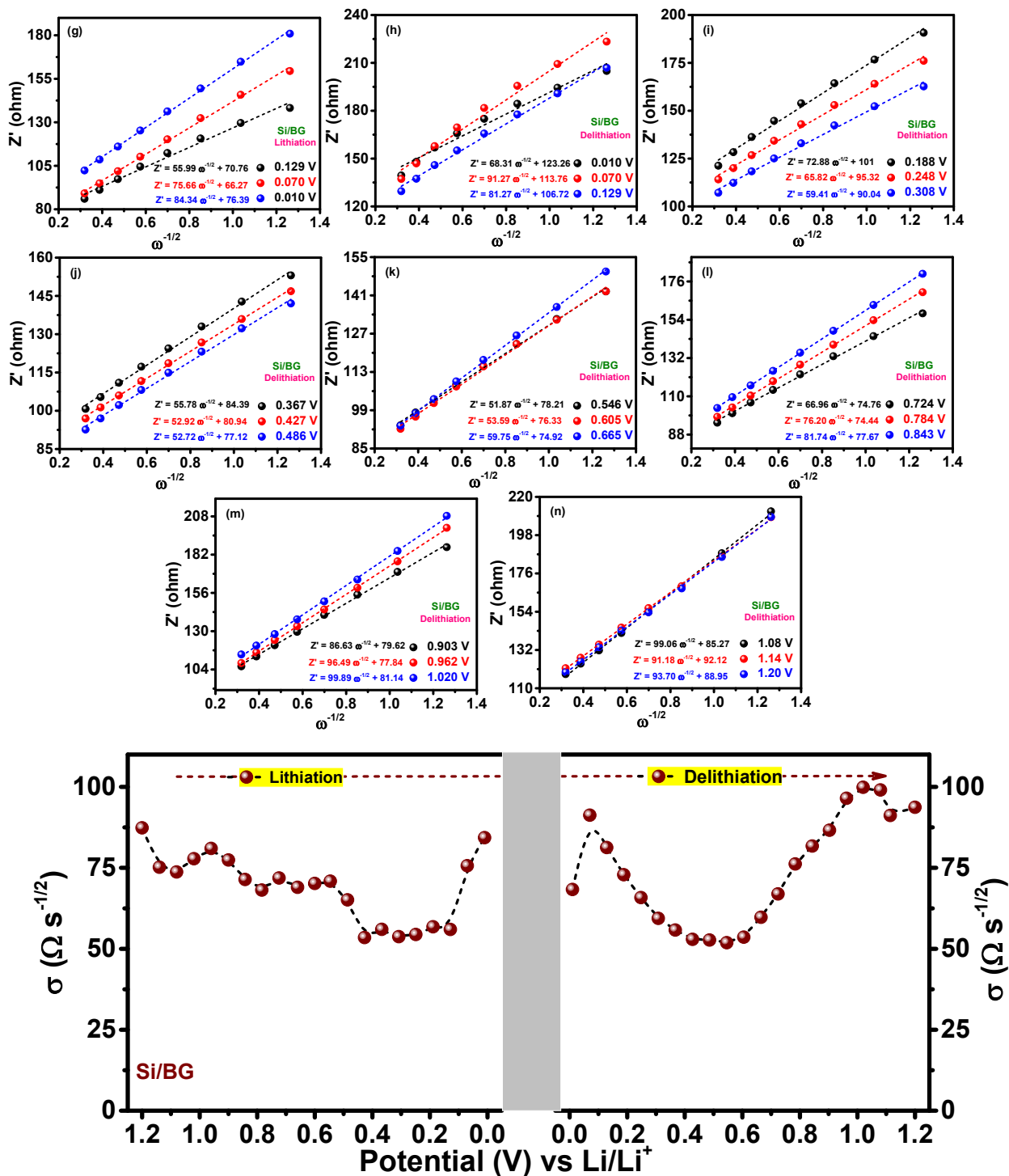
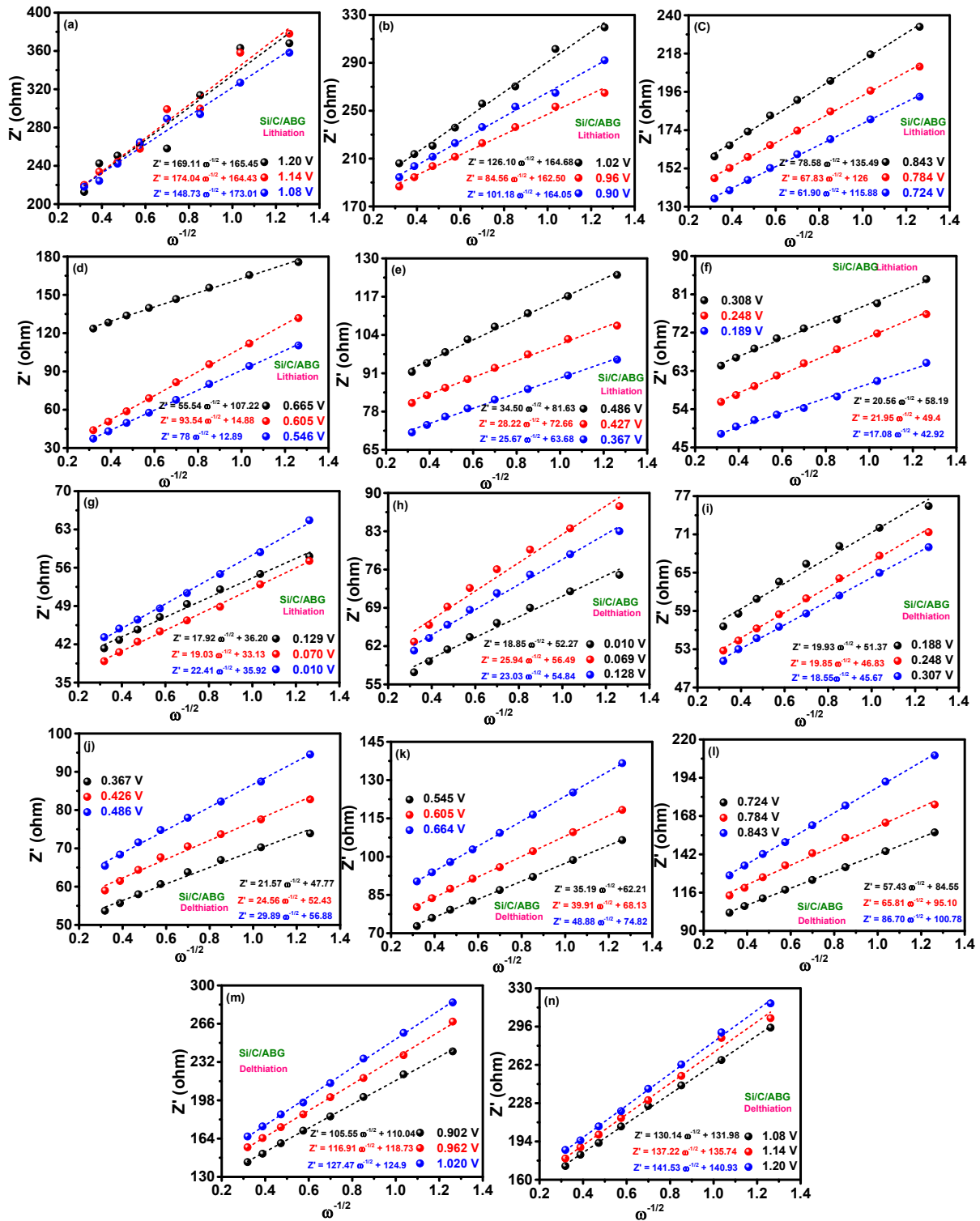


Figure S9. The Warburg plots for lithiation (a-g) and delithiation (h-n), construed from low frequency region of each Nyquist plots in DEIS spectra (Figure S6) of Si/BG, post rate

study (after ~65th cycle). (o) Warburg coefficient, σ , variation of Si/BG anode over lithiation – delithiation potential window, deduced from the slope of Warburg plots.



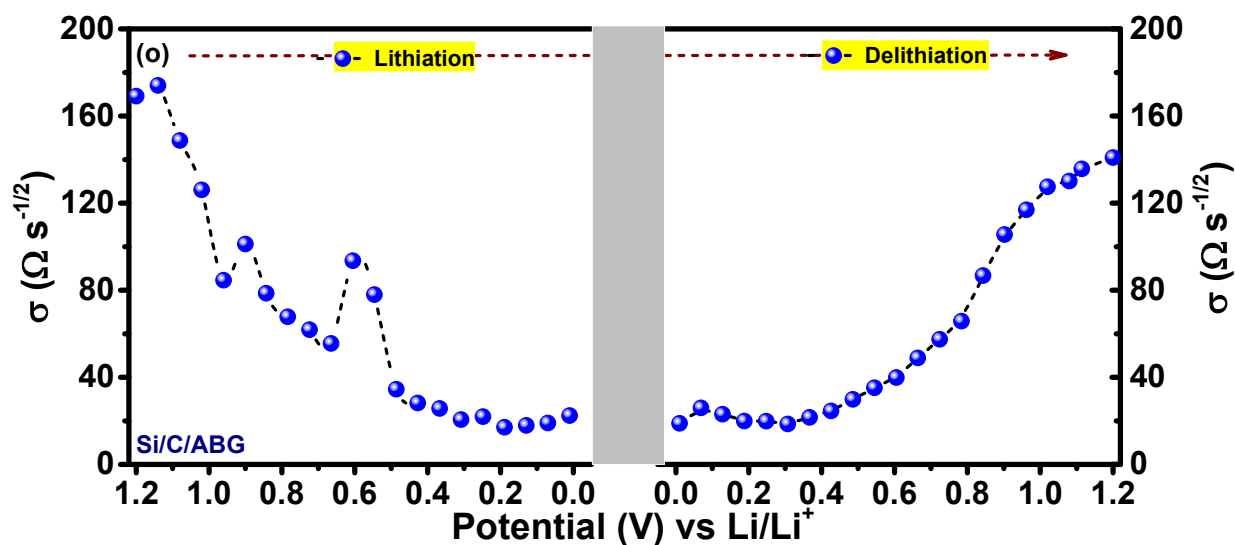


Figure S10. The Warburg plots for lithiation (a-g) and delithiation (h-n), construed from low frequency region of each Nyquist plots in DEIS spectra (Figure S6) of Si/C/BG, post rate study (after $\sim 65^{\text{th}}$ cycle). (o) Warburg coefficient, σ , variation of Si/C/BG anode over lithiation – delithiation potential window, deduced from the slope of Warburg plots.

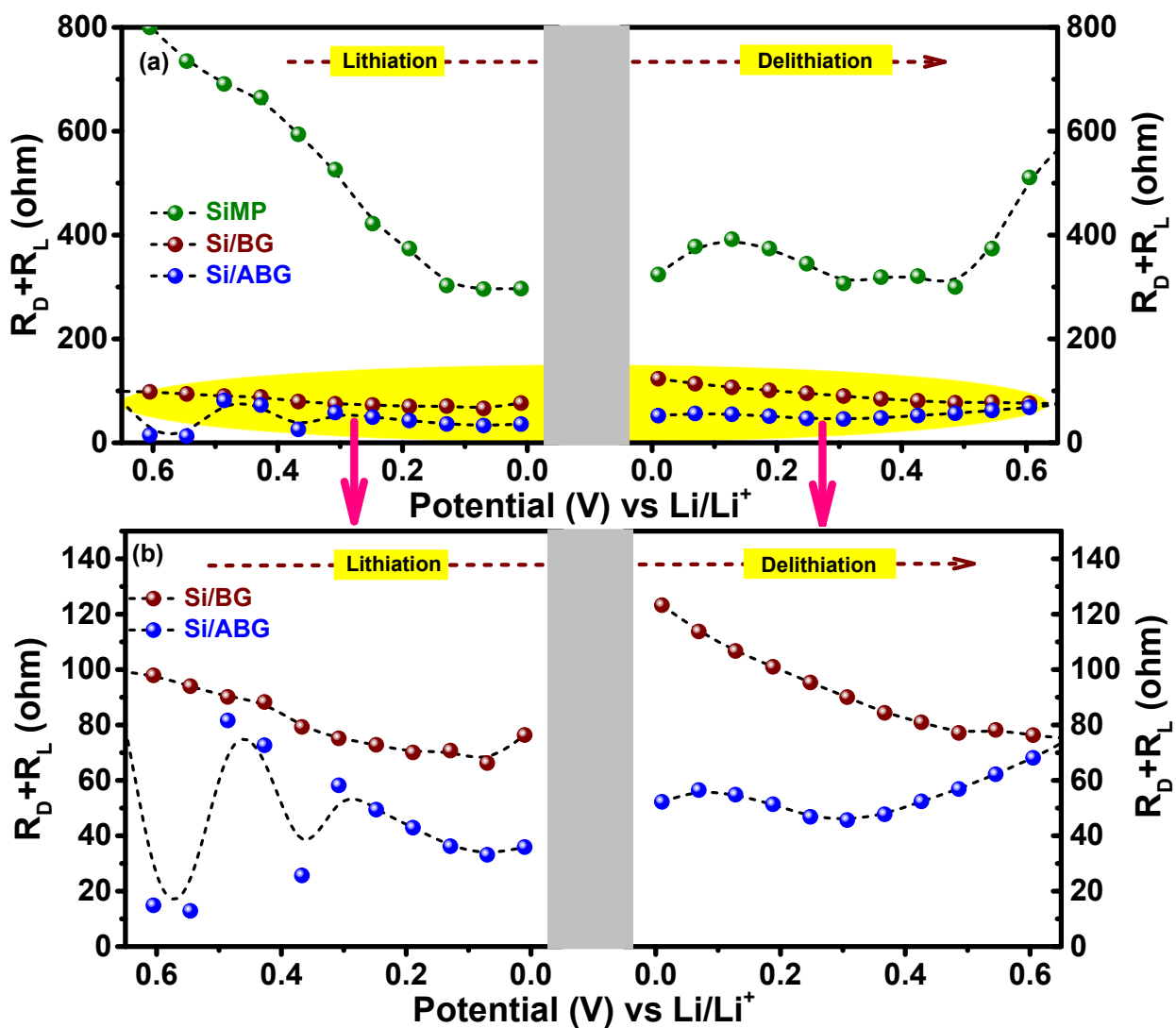


Figure S11. The variation of overall total resistance ($R_D + R_L$) of SiMP, Si/BG and Si/C/ABG over lithiation-delithiation potential window. The overall resistance of SiMP or Si/BG or Si/C/ABG were obtained from the intercept of respective Warburg plots Figure S7, Figure S8 and Figure S9, respectively.

Table S6. Comparative reversible storage ability performance of some of the Si based composite anode materials used in LIB studies in recent years.

Anode material	Reversible lithiation capacity (mAh/g)	After n th cycle	Current rate (mA/g)	Reference
Si/MWNTs	700	40	500	Chem. Commun., 46 (2010), 9149-9151
FeSi ₂ /Si@C composite	940	200	100	ACS Appl. Mater. Interfaces, 4 (2012), 3753-3758
Si-porous carbon layers and graphene layers (Si-C/G)	760	100	200	Carbon, 84 (2015), 434-443
Si/mesoporous C composite	1018	100	500	J. Mater. Chem. A, 2 (2014), 9751-9757
Si/void/porous carbon composite	980	80	100	Electrochim. Acta, 125 (2014), 206-217
Si/void/SiO ₂ /void/C nanostructures	956	430	460	Sci. Rep., 5 (2015), 10908
Carbon coated micro-sized porous Si	1041	300	500	Nano Energy, 11 (2015), 490-499
Si@C-rGO	930	400	300	Adv. Energy Mater., 6 (2016), 1600904
SiOC	980	400	180	<i>Energy Storage Mater.</i> , 2021, 35 , 130–141
Pre-lithiated SiO	906	100		Nano Lett., 2016, 16, 282
SiO ₂ /N	672	50		Adv. Funct. Mater., 2017, 28, 1704561
SiO _x @GO	740	1000		Adv. Mater., 2018, 30,

				1707430
Double core-shell Si/G/C	847	500	0.2 C	Surface & Coatings Technology 387 (2020) 125528 2
Si@G electrodes	850	100	250	Molecules2020,25, 2494
SiNPs-C/G	505	500	100	ACS Appl. Mater. Interfaces2019, 11, 35809–35819
Si/C-AG	445	200	500	Electrochimica Acta 337 (2020) 135687
<i>Si/C/ABG</i>	<i>1017</i>	<i>775</i>	<i>750</i>	<i>Present study</i>
	<i>1572</i>	<i>260</i>	<i>150</i>	

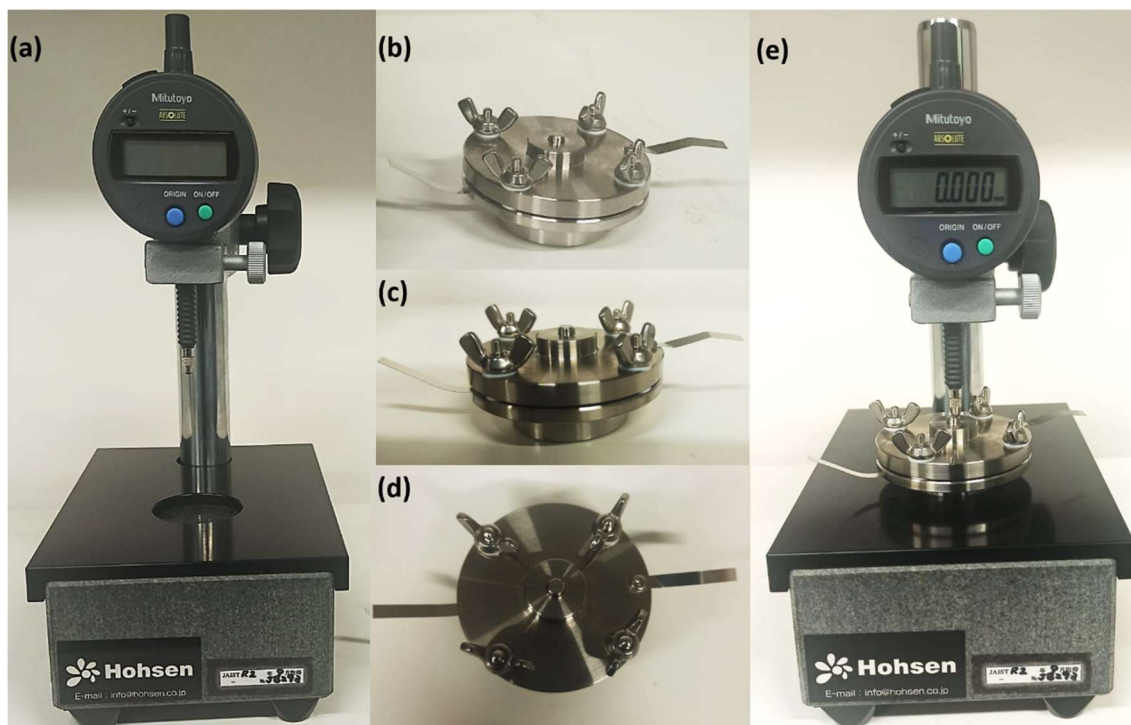


Figure S12. Optical photographs of (a) digital meter stand and (b-d) HS cell. (e) The complete unified arrangement of digital meter coupled HS cell ready for electrochemical screening. Prior to starting of each electrochemical screening, the origin was set to zero.

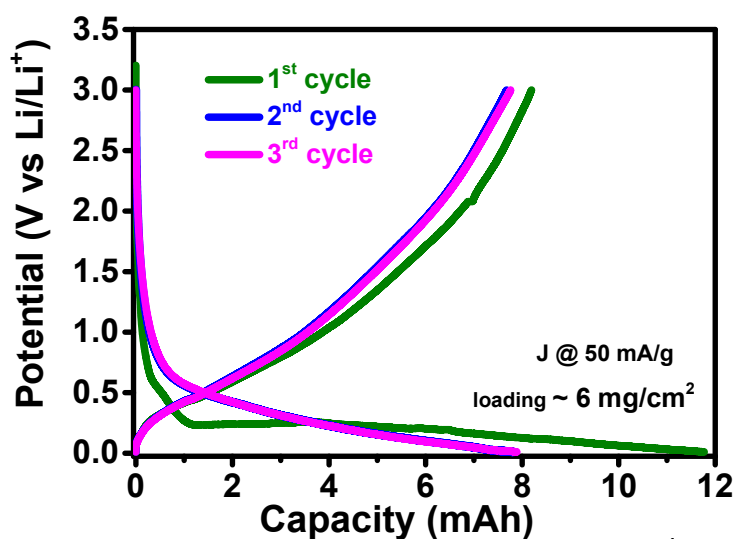


Figure S13. Lithiation-delithiation voltage profiles at $J=50$ mA/g on Si/C/ABG anodic half-cell (CR2025 coin cell). The anode material (Si/C/ABG) loading was ~ 6 mg/cm².



Figure S14. The optical photo graphs of (a,b) LED arrangement, cell holders and a pair of NCA (cathode) // Si/C/ABG (anode) based full-cells. (c) Powering the LED arrangement using NCA // Si/C/ABG based full-cells.

Table S7. The energy density at different current rate (with respect to anode loading) of NCA//Si/C/ABG based full cell, deduced from Figure 8 in main text.

Current rate (mA/g)	Full cell energy density (Wh/kg)
75	~ 230 (1 st cycle),
150	~ 171 (14 th cycle),
300	~ 148 (21 st cycle),
450	~ 132 (28 th cycle),
750	~ 112 (35 th cycle),

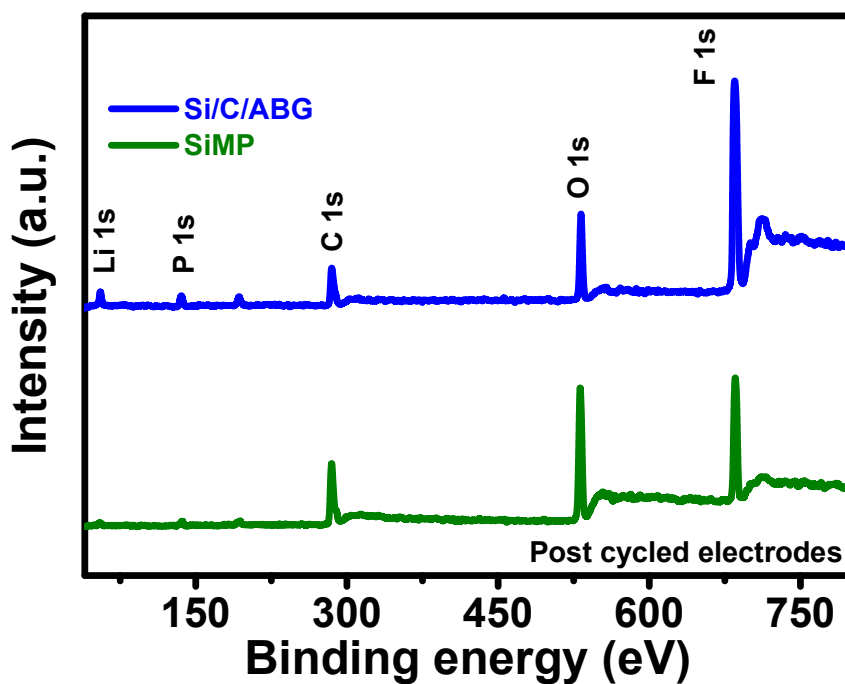


Figure S15. The ex-situ wide XPS spectra on cycled (after rate study, post ~65th cycle) SiMP and Si/C/ABG anodes.

References

- 1 H. Lee, S. M. Dellatore, W. M. Miller and P. B. Messersmith, *Science (80-.)*, 2007, **318**, 426–430.
- 2 R. Nandan, N. Takamori, K. Higashimine, R. Badam and N. Matsumi, *J. Mater. Chem. A*, 2022 , DOI:10.1039/D1TA08516F.
- 3 R. Nandan, P. Pandey, A. Gautam, O. Y. Bisen, K. Chattopadhyay, M. M. Titirici and K. K. Nanda, *ACS Appl. Mater. Interfaces*, 2021, **13**, 3771–3781.
- 4 R. Nandan, A. Gautam and K. K. Nanda, *J. Mater. Chem. A*, 2017, **5**, 20252–20262.
- 5 C. Sun, Y. J. Wang, H. Gu, H. Fan, G. Yang, A. Ignaszak, X. Tang, D. Liu and J. Zhang, *Nano Energy*, 2020, **77**, 105092.
- 6 R. Nandan, N. Takamori, K. Higashimine, R. Badam and N. Matsumi, *J. Mater. Chem. A*, 2022 , DOI:10.1039/d1ta08516f.